μ-EXAFS, μ-XRF, and μ-PL Characterization of a Multi-Quantum-Well Electroabsorption Modulated Laser Realized via Selective Area Growth

*Lorenzo Mino, Diego Gianolio, Giovanni Agostini, Andrea Piovano, Marco Truccato, Angelo Agostino, Stefano Cagliero, Gema Martinez-Criado, Francesco d' Acapito, Simone Codato, and Carlo Lamberti**

In the past few years, strong efforts have been devoted to improving the frequency of optical-fiber communications. In particular, the use of a special kind of integrated optoelectronic device called an electroabsorption modulated laser (EML) allows communication at 10 Gb s^{-1} or higher over long propagation spans (up to 80 km). Such devices are realized using the selective area growth (SAG) technique and are based on a multiple quantum well (MQW) distributed-feedback laser (DFB) monolithically integrated with a MQW electroabsorption modulator (EAM). Since the variation in the chemical composition between these two structures takes place on the micrometer scale, in order to study the spatial variation of the relevant parameters of the MQW EML structures, the X-ray microbeam available at the ESRF ID22 beamline is used. The effectiveness of the SAG technique in modulating the chemical composition of the quaternary alloy is proven by a micrometer-resolved X-ray fluorescence (μ-XRF) map. Here, reported micrometer-resolved extended X-ray absorption fine structure (μ-EXAFS) spectra represent the state of the art of μ-EXAFS achievable at third-generation synchrotron radiation sources. The results are in qualitative agreement with X-ray diffraction (XRD) and micrometer-resolved photoluminescence (μ-PL) data, but a technical improvement is still crucial in order to make μ-EXAFS really quantitative on such complex heterostructures.

L. Mino, D. Gianolio, Dr. G. Agostini, Dr. A. Piovano, Prof. C. Lamberti,
Department of Inorganic
Materials and Physical Chemistry
NIS Centre of Excellence and INSTM unit
University of Turin
Via P. Giuria 7, I-10125 Turin, Italy
E-mail: carlo.lamberti@unito.it

Dr. M. Truccato, Dr. S. Cagliero
NIS Centre of Excellence
Department of Experimental Physics
University of Turin
Via P. Giuria 1, I-10125, Turin, Italy

Dr. A. Agostino, Dr. S. Cagliero
NIS Centre of Excellence
Department of General and Organic Chemistry
University of Turin
C.so Massimo D'Azeglio 48, I-10125, Turin, Italy

Dr. G. Martinez-Criado
ESRF, 6 rue Jules Horowitz
BP220, F-38043, Grenoble CEDEX, France

Dr. F. d'Acapito
CNR-IOM-OGG c/o ESRF, GILDA-CRG, 6 rue Jules Horowitz, BP220,
F-38043, Grenoble CEDEX, France

S. Codato
Avago Technologies Italy S.r.l.
Torino Technology Centre
Via G. Schiaparelli 12, 10148 Turin, Italy

DOI: 10.1002/smll.201001229

© 2011 Wiley-VCH Verlag GmbH & Co. KGaA, Weinheim

1. Introduction

In the field of semiconductor bandgap engineering, the frontier of research is represented by 1D- and 0D-confined systems, usually named quantum wires[1–6] and quantum dots, respectively.[7,8] Nevertheless, for several practical reasons, the economical market of III–V quantum lasers is still dominated by 2D-confined quantum well and multi quantum well (MQW) heterostructures that are currently widely used in optical communication systems.[9–17] They are deposited on suitable substrates using appropriate growth techniques, like molecular beam epitaxy (MBE)[16] or metal–organic vapor-phase epitaxy (MOVPE).[12,15,18] The MOVPE growth process starts from group III (metal organics) and group V (hydrides) precursors that are thermally decomposed and subsequently deposited uniformly on the substrate, rebuilding the crystal lattice layer by layer with the desired composition. In this way, the device can perform only one function (e.g., photodiode, light-emitting diode, waveguide, laser, amplifier, modulator) but, in modern optoelectronic devices, the integration of two different functions in the same chip is often required.

In order to join functions, in the past, external connections were realized between discrete devices; however, this approach suffered from many disadvantages: high dimensions of the final device, high cost, high sensitivity to temperature, and relatively low efficiency of the coupling, resulting in a high fraction of photon loss. Excellent results in the development of monolithic integration have been reached with the selective area growth (SAG) technique.[19–27]

SAG exploits the perturbation of the growth fluxes induced by a dielectric mask (usually SiO_2). When the metal–organic precursors collide with the dielectric mask, they are deflected and they can desorb or migrate through the unmasked semiconductor regions, where the growth can start. In this way, the reactive species coming from the gas phase are enriched by those deflected by the mask and a different material is obtained with respect to the unmasked region. Since the reactive species have different diffusion lengths,[28] the result is a variation in composition and thickness of semiconductors grown near (SAG region) and far (FIELD region) from the mask (**Figure 1**a).

One of the most promising applications of this technique are electroabsorption modulated lasers (EML)[29–31] obtained by monolithic integration of an electroabsorption modulator (EAM) with a distributed feedback laser (DFB). They are particularly interesting for long-distance (up to 100 km) communications at high frequency (10 Gb s^{-1}); in fact, a directly modulated DFB laser is limited by its positive chirp.[32] The use of external modulation takes advantage of the zero or even negatively chirped pulses generated by the EAM and, using a constantly injected DFB laser, exploits the limited fiber attenuation of the third window at 1550 nm. A voltage modulation at 10 GHz, applied to the EAM, switches it between an opaque and a transparent state by means of the Stark effect[33] (Figure 1b) and ensures the modulation of the DFB laser emission.

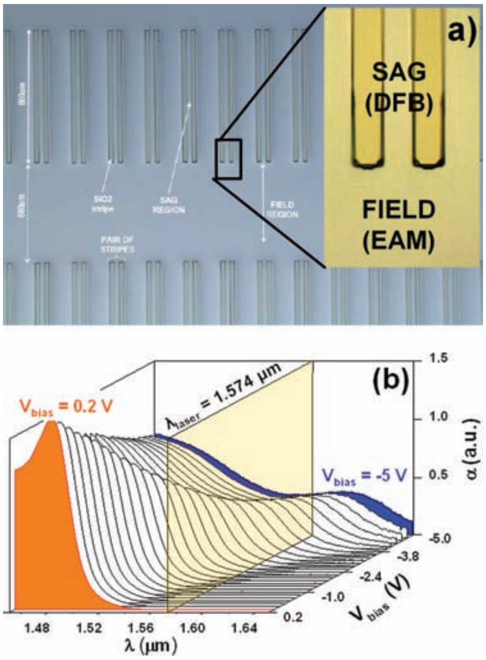

Figure 1. a) Optical micrograph of an InP substrate patterned with SiO_2 stripes, which allow SAG growth. b) Quantum Stark effect measured on the electroabsorption modulator (EAM) showing the progressive transition from opaque to transparent to the light emitted by the distributed-feedback (DFB) laser (vertical yellow plane).

In this Full Paper, we studied a SAG EML based on an $Al_{xw}Ga_{yw}In_{1-xw-yw}As/Al_{xb}Ga_{yb}In_{1-xb-yb}As$ (compressive-strained well/tensile-strained barrier) MQW structure grown on InP by MOVPE. We chose a mask with 30-μm-wide SiO_2 stripes and 30-μm opening widths between them. Using 800-μm-long stripes and a 600-μm-long FIELD zone (Figure 1a), two devices per couple of stripes can potentially be obtained after cleavage and processing (about 20 000 per 2 inches of InP substrate; 1 inch = 2.54 cm). This quaternary alloy is less diffuse with respect to $In_{xw}Ga_{1-xw}As_{yw}P_{1-yw}/In_{xb}Ga_{1-xb}As_{yb}P_{1-yb}$ because of the problem of Al oxidation during the synthesis but has better temperature behavior and modulation speed.[28,34]

Until now, trial-and-error procedures were adopted for the choice of growth parameters since the micrometer-variation of composition and thickness inherent to the SAG technique requires high-brilliance X-ray microbeams[35] in order to perform a proper characterization. These features are not achievable with conventional laboratory X-ray sources, therefore we used the 5.3–μm × 1.7–μm X-ray beam available at the ID22 beamline[36] of the European Synchrotron Radiation Facility (ESRF).

Although focused on a very specific class of materials (SAG-grown III–V heterostructures for optoelectronic devices[37–42]), the present contribution highlights the important improvements achieved in both beam focusing and beam stability that could be successfully applied in several frontier topics, in materials science, geology, archaeometry, environmental sciences, biology, neuroscience, and medicine. Without any presumption of exhaustivity, a small list of selected applications in different fields follows:

- Materials science: Determination of doping profiles and doping local environments in semiconductor films;[43–47] spatial determination of complex intermetallic phases in multicrystalline silicon doped with transition metals;[48] study of composition and Cu oxidation-state gradient in $Bi_2Sr_2CaCu_2O_{8+\delta}$ (Bi-2212) superconducting whiskers;[49,50] spatial determination of residual strain gradients in composite materials[51,52] or in externally bent semiconductors;[53] investigation of the local strain tensor of different heteroepitaxial layers with submicrometer resolution in oxide films grown on metal substrates.[54]

- Geology: Speciation of dilute contaminants in natural sediments[55–60] and in fluid inclusions;[61] selective detection of Fe and Mn species at mineral surfaces in weathered granite.[62]
- Archaeometry: Single-grain investigation in ancient Egyptian makeup.[63]
- Environmental sciences: Characterization of PM2.5–PM10 pollutant particles in the ambient air of Shanghai city by analyzing individual particles.[64,65] PM = particulate matter; the notation PM10 is used to describe particles of 10 µm or less and PM2.5 represents particles less than 2.5 µm in aerodynamic diameter.
- Biology: Biomineralization of Au nanoparticles in metallophillic bacteria;[66] space-resolved analysis of the hierarchical structure of biological tissues;[67] investigation of the distribution of elements in snail shells.[68]
- Neuroscience: Determination of Fe oxidation state in a single neuron.[69]
- Medicine: Distribution of trace elements and determination of Cu oxidation state in breast tumor tissue.[70]

2. Results and Discussion

2.1. Laboratory Micrometer-resolved Photoluminescence Investigation

As grown wafer was first examined by micrometer-space-resolved photoluminescence (μ-PL) spectroscopy in order to verify if the grown material had the optimal energy gap for DFB and EAM operation and to obtain information about the growth quality.[71,72] We adopted a sampling with a 15-µm resolution along a line parallel to the SiO_2 stripes and equidistant to them (the so-called "Y-line").

Figure 2 highlights that the DFB laser (SAG region) emits at the desired wavelength for third-window communications and that the EAM (FIELD region) has an higher energy gap and so is transparent to the radiation emitted by the laser, as shown in Figure 1b, but the application of a negative potential (usually –2 V) switches it to opaque.

Comparing the PL spectra along the Y-line, a progressive relative degradation of the crystalline quality of the MQW is appreciable by moving from FIELD to SAG, where the PL intensity is lower and the full width at half maximum (FWHM) is larger (see Figure 2). The phenomenon is related to a lack of strain compensation, to a higher growth rate, and to the interference of precursors fluxes in the SAG region and has recently been highlighted on similar SAG heterostructures grown adopting a narrower SiO_2 stripes (20 µm).[41]

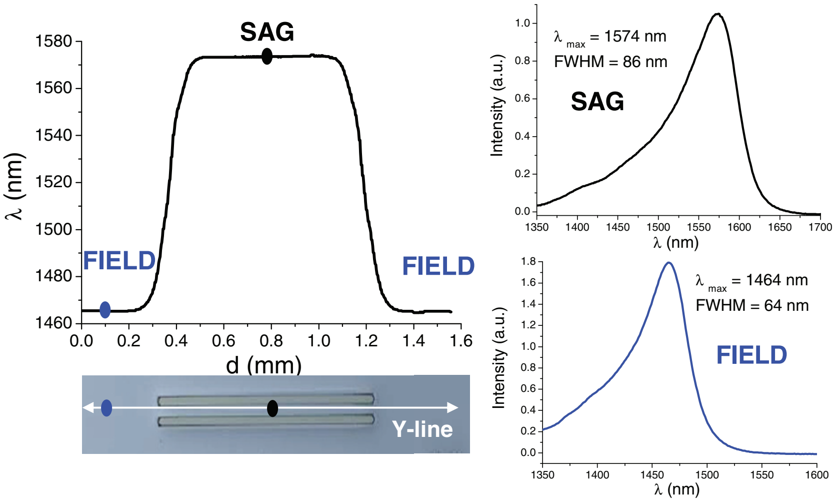

Figure 2. Left: maximum of the emission wavelength for each PL spectrum versus position along the Y-line. Right: complete PL spectra for two points located in the SAG and FIELD regions, which are highlighted in the optical micrograph.

2.2. Synchrotron Radiation μ-X-Ray Fluorescence Investigation

Normally, the characterization of these kind of structures is performed by combining PL with high-resolution X-ray diffraction (XRD)[38,72–78] but, in the present work, we adopted a different exhaustive approach. We carried out an X-ray fluorescence (XRF) study to investigate the spatial variation of the growth thickness and of the chemical composition, which are the key parameters for optimizing the growth process and therefore the device performance. From **Figure 3**, it is possible to see that the Ga K_α- and As K_β-related counts are higher in the SAG region owing to the material enrichment caused by the SiO_2 stripes. The In $L_{\alpha,\beta}$ map is dominated by the emission coming from the InP substrate: in fact, the signal is higher where the SiO_2 stripes are present, since they are less effective than the MQW structures in reabsorbing the emission coming from the substrate. Unfortunately, the absorption from air and from the detector Be window prevented us from collecting the Al $K_{\alpha,\beta}$ fluorescence at 1.5 keV: this could be overcome in the future by using a He atmosphere. The knowledge of the Al counts could have allowed us to perform a complete quantitative analysis, as recently proved for ternary InGaAs/InP grown with the SAG technique.[42]

The effectiveness of SAG technique in modulating the chemical composition of the quaternary alloy is proven by the map reporting the Ga/As count ratio (Figure 3), in which

© 2011 Wiley-VCH Verlag GmbH & Co. KGaA, Weinheim

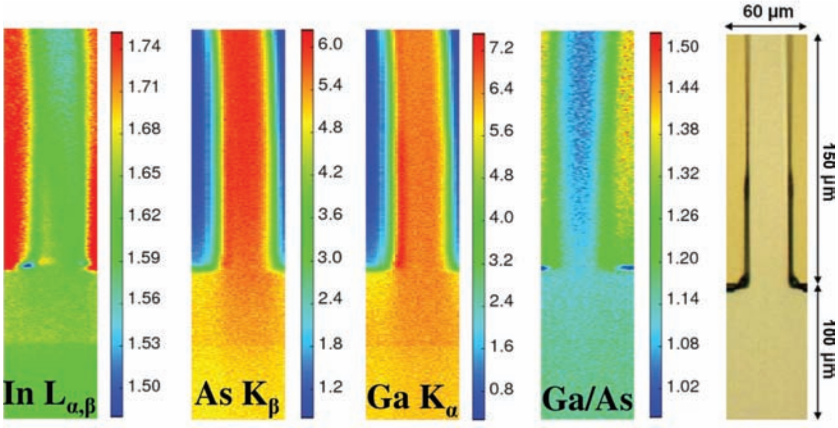

Figure 3. Spatial maps of the fluorescence counts of the principal element's lines (beam energy: 17 keV). The optical micrograph on the right shows the area that has been sampled. The use of As-K_β emission in place of the As-K_α was due to the fact that the As-K_α has a partial superimposition with Ga-K_β.

a gradient in the average well/barrier chemical composition is clearly visible. Since the Ga/As ratio is lower in the SAG region than in the FIELD, we can assert that the average Ga content of the MQW structure progressively increases along the Y-line by moving from SAG to FIELD. This is due to the SAG effect that exploits the shorter diffusion length of In (D/k, where D is the diffusion coefficient and k is the rate of adsorption on the surface) with respect to that of Ga and Al.[24,28,41,79]

2.3. Synchrotron Radiation μ-X-Ray Absorption Fine Structure Investigation

X-ray absorption fine structure (XAFS) has been often applied to semiconductor heterostructures and nanostructures in order to understand the relationship between local atomic structure and physical properties.[74,80–94] In our case, measurements at both Ga and As K-edges were performed in the SAG, interface, and FIELD regions: the higher intensity of the non-normalized XAFS spectrum in the SAG region (**Figure 4**) reflects the increased quantity of material deposited between the SiO_2 stripes, as already discussed in the XRF analysis.

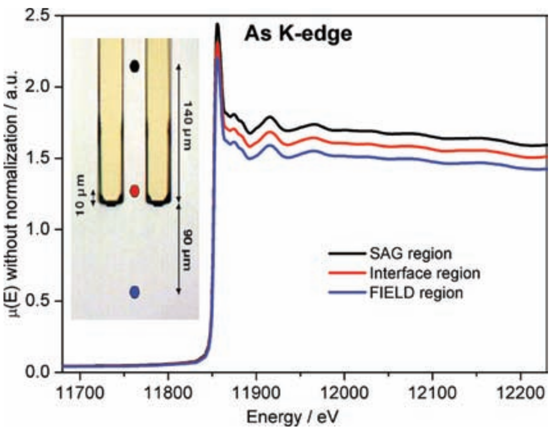

Figure 4. Comparison between the non-normalized absorption coefficients collected in the three points marked by colored dots in the optical micrograph.

The change from micrometer-resolved XRD or XRF to micrometer-resolved XAFS basically requires the modification of the positions of the monochromator and undulator simultaneously from fixed to variable values.[95] The spectroscopy implies an energy scan over the 1000 eV range by driving the theta motor of the monochromator. It is consequently extremely difficult to keep an X-ray μ-beam in the same point within a sub-micrometer precision in order to irradiate the same portion of the sample during the entire energy range of an XAFS spectrum.[96] The longer the energy scan, the greater are the technical difficulties to avoid any drift of the focal spot based on Kirkpartrick–Baez (KB) mirrors[97] working at grazing incidence (≈3.5 mrad). Nevertheless, the achromaticity of the KB mirrors guarantees a much higher beam stability along an energy scan than that obtained with chromatic optics, like zone plates or Fresnel lenses.

These arguments explain why in the literature one can find several micrometer-resolved X-ray absorption near-edge structure (μ-XANES) results,[44,49,50,63,66,69,70,98] where only a few tens of electron-volts are scanned across the edge, whereas papers reporting micrometer-resolved extended XAFS (μ-EXAFS) data, requiring an energy scan of several hundreds of eV, are much more rare.[45,46,48,55–60,96,99,100] In the cited studies, an XRF micrometer-resolved map evidenced the presence of domains in the samples, characterized by different chemical or phase natures, with a size in the 10–100 µm range. Inside each domain, the sample was homogeneous, so that small fluctuations of the μ-beam inside a single domain would not heavily affect the spectroscopic result.

In the present case, as evidenced by the μ-XRF investigation (see Figure 3), we are dealing with a continuous change in the chemical composition of the sample. This sample characteristic, combined with the difficulty in keeping the X-ray beam in the same position with sub-micrometer resolution along the energy scan, justifies the relatively short k-range in the EXAFS spectra, as reported in Figure 4, that is exploitable for the data analysis. However, this experiment represents the state of the art in micrometer EXAFS on samples showing inhomogeneities in the micrmeter range. The differences in the EXAFS spectra collected in the three regions are very small, so we decided to analyze only the two data sets corresponding to the extreme conditions (i.e., collected in the SAG and FIELD regions).

The short k range available for the analysis and the high number of parameters to be optimized (the As is surrounded by three different cations in its first coordination shell) led us to try to maximize as much as possible the available data set while reducing the number of optimized parameters.

The former goal is achieved by doing a combined fit of Ga and As K-edge spectra (**Table 1**; **Figure 5** and **Figure 6**). In fact, a double-edge EXAFS data analysis (see **Table 2**) allows

Table 1. Summary of the parameters optimized in the fitting of the EXAFS data (Figure 5 and Figure 6) on the SAG and FIELD regions of the quaternary heterostructure. A co-refinement approach on As and Ga K-edges was adopted. The fits were performed over k^3-weighted FTs of the $\chi(k)$ functions using the following intervals in k and R spaces: 3.0–9.0 Å^{-1} and 1.0–3.2 Å for As K-edges, 3.0–10.8 Å^{-1} and 1.0–4.3 Å for Ga K-edges.

Parameter	SAG	FIELD
$R_{\text{As-Ga}}$ [Å]	2.469 ± 0.007	2.463 ± 0.005
$\Delta R_{\text{As-Ga}}$ [Å]	0.021 ± 0.007	0.015 ± 0.005
$R_{\text{As-In}}$ [Å]	2.60 ± 0.02	2.60 ± 0.02
$\Delta R_{\text{As-In}}$ [Å]	−0.02 ± 0.02	−0.02 ± 0.02
$R_{\text{As-Al}}$ [Å]	2.49 ± 0.11	2.48 ± 0.11
$\sigma^2_{\text{As-Ga}}$ [Å^2]	0.006 ± 0.002	0.005 ± 0.002
$\sigma^2_{\text{As-In}}$ [Å^2]	0.008 ± 0.003	0.007 ± 0.003
$\sigma^2_{\text{As-Al}}$ [Å^2]	0.010 ± 0.004	0.008 ± 0.004

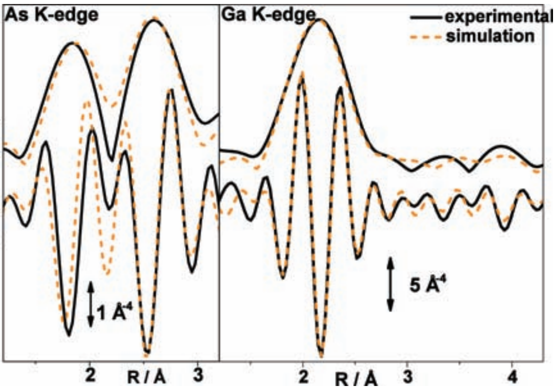

Figure 6. k^3-weighted, phase-uncorrected, Fourier-transform modulus and imaginary part of Ga and As K-edges, performed in the FIELD region. For the fit a co-refinement approach was adopted using the following intervals in k and R spaces: 3.0–9.0 Å^{-1} and 1.0–3.2 Å for As K-edges, 3.0–10.8 Å^{-1} and 1.0–4.3 Å for Ga K-edges.

the significance of the results to be increased relative to the analysis obtained with a standard single-edge analysis because the parameters of the same structural model are refined on two independent sets of experimental data. In particular, the co-refined parameters were the As–Ga bond length ($R_{\text{As-Ga}}$) and the related Debye–Waller factor ($\sigma^2_{\text{As-Ga}}$)

The latter goal was achieved by imposing a high number of constraints on the EXAFS parameters of the different shells. In particular, the relative fraction of the three cations in the first shell of As and in the second shell of Ga was fixed according to XRD data[101] ($Al_{0.135}Ga_{0.310}In_{0.555}As$ for SAG and $Al_{0.148}Ga_{0.322}In_{0.531}As$ for FIELD); the edge energies and S_0^2 parameters were set to the values obtained from the analysis of the binary reference samples (see Table 2 and **Figure 7**) and the second-shell distances were left unchanged with respect to the virtual-crystal approximation (VCA) values.[90,102]

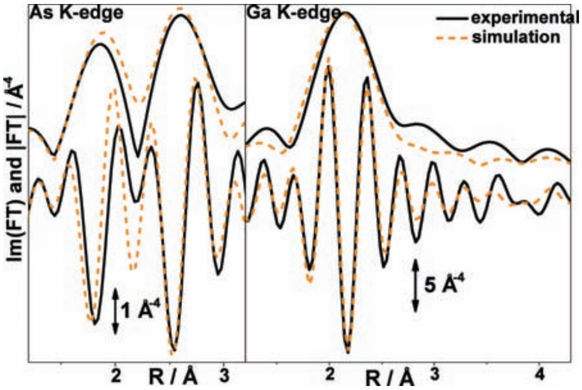

Figure 5. k^3-weighted, phase-uncorrected, Fourier-transform (FT) modulus and imaginary part of Ga and As K-edges, performed in the SAG region. For the fit a co-refinement approach was adopted using the following intervals in k and R spaces: 3.0–9.0 Å^{-1} and 1.0–3.2 Å for As K-edges, 3.0–10.8 Å^{-1} and 1.0–4.3 Å for Ga K-edges. It is worth noticing that in the As K-edge FT, the joint As–Al, As–Ga, and As–In first-shell contribution (1.5–3.0 Å) exhibits a double-peak-featured shape. This "strange" feature depends on the k interval used to calculate the FT and is typical of first-shell scattering atoms with high Z numbers (In, in our case), of which the scattering amplitudes are modulated in k range.[84,104]

The quality of the data allowed us to perform a fit up to the second coordination shell for the Ga K-edge spectra, while only the first shell could be optimized from the As K-edge data. In conclusion, we performed a six-parameter fit (see Table 1), where phases and amplitudes have been calculated using the FEFF8.4 code using as the input a cluster obtained on the basis of the VCA approximation.[90]

This procedure allowed us to estimate the variation of the first-shell distances in the quaternary alloy with respect to the bulk binary compounds, which appears to be comparable to what has been observed in $In_xGa_{1-x}As$ ternary alloys.[90,103] The optimized Debye–Waller factors (Table 1) exhibit significantly higher values with respect to those obtained in the binary-model compounds (Table 2), reflecting the higher static disorder of the quaternary heterostructure.

From the summary of the results reported in Table 1, the following considerations can be drawn: i) We observed a stretching of the As–Ga first-shell bond distances and a contraction of the As–In first-shell distances with respect to

Table 2. Summary of the parameters optimized in the fitting of the EXAFS data (Figure 7) on the binary reference samples. The fits were performed over k^3-weighted FTs of the $\chi(k)$ functions performed in the 2.0–18.0 Å^{-1} interval. In R-space, we employed the 1.0–3.0 Å range for both As K-edges and the 1.0–4.3 Å range for the Ga K-edge.

Parameter	InAs (As K-edge)	GaAs (As K-edge)	GaAs (Ga K-edge)
ΔE_0 [eV]	3.9 ± 0.9	3.2 ± 0.6	2.1 ± 0.8
S_0^2	0.94 ± 0.08	1.03 ± 0.04	0.92 ± 0.05
$R_{\text{As-Ga}}$ [Å]	–	2.445 ± 0.002	2.443 ± 0.003
$R_{\text{As-In}}$ [Å]	2.622 ± 0.003	–	–
$\sigma^2_{\text{As-Ga}}$ [Å^2]	–	0.0042 ± 0.0002	0.0039 ± 0.0002
$\sigma^2_{\text{As-In}}$ [Å^2]	0.0045 ± 0.0003	–	–
$R_{\text{Ga-Ga2}}$ [Å]	–	–	4.000 ± 0.009
$\sigma^2_{\text{Ga-Ga2}}$ [Å^2]	–	–	0.0124 ± 0.0009

© 2011 Wiley-VCH Verlag GmbH & Co. KGaA, Weinheim

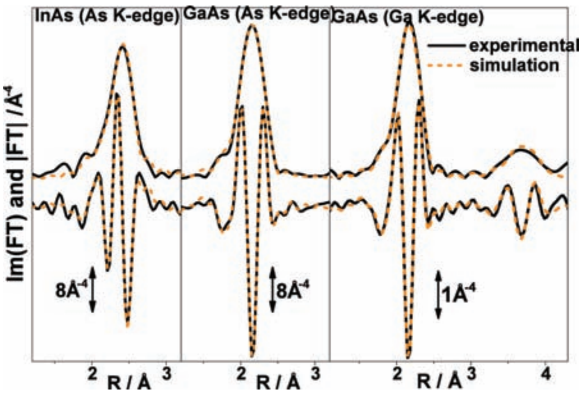

Figure 7. k^3-weighted, phase-uncorrected, Fourier-transform modulus and imaginary part of Ga and As K-edges, for the GaAs and InAs reference binary samples: experimental curves in black, fits in orange.

the binary compounds InAs and GaAs (see Table 2). These distances are in agreement with experimental[86] and theoretical[105] data on strained $In_{0.60}Ga_{0.40}As$ alloys on InP. ii) The relatively low concentration of Al, combined with its smaller (compared to that of Ga and In) scattering power, results in an unreliable determination of the As–Al distance, accompanied with an error as high as 0.1 Å. iii) The observed trends are those expected as the $\Delta R_{\text{As-Ga}}$ is higher in the SAG than in the FIELD region and a higher structural disorder (monitored by the σ^2 values) is observed in the SAG region, confirming the PL evidence (see Figure 2); however, the quality of the data results in error bars that are too high to allow us to discriminate safely between the SAG and FIELD regions.

3. Conclusion and Perspectives

We have presented a micrometer-resolved PL, XRF, and EXAFS study on an $Al_xGa_yIn_{1-x-y}As$ heterostructure grown on an InP(001) substrate by the SAG technique, which represents the core of EAM laser devices employed in high-frequency optical-fiber communications.

The following results have been achieved: i) μ-PL highlighted that the DFB laser (SAG region) emits at the desired wavelength for third-window communications and that the EAM (FIELD region) has an higher energy gap and so is transparent to the radiation emitted by the laser, switching to opaque by the Stark effect with the application of a negative potential. ii) μ-XRF directly proved the effectiveness of the SAG technique in modulating the chemical composition of the quaternary alloy. The XRF map reporting the ratio between Ga and As clearly evidenced the composition gradient between the SAG and FIELD regions, due to the shorter diffusion length (D/k) of In with respect to that of Ga and Al. iii) μ-EXAFS results (namely the R_{InAs} and R_{GaAs} parameters) are in agreement with the presence of a strained alloy at about 60% In content, presenting a qualitative agreement with XRD and μ-PL data. Technical improvements are still needed in order to improve the accuracy of μ-EXAFS so as to permit a distinction between the different zones of the device.

It is relevant to note that the study was not performed on an academic prototype but directly on a MQW growth obtained with the SAG technique from which up to 20 000 EMLs operating at 10 Gbit s^{-1} in the third fiber-optic window (1550 nm) can be obtained after processing. Until now, such lasers, available on the market in the last few years, were achieved by epitaxial techniques where the growth parameters were optimized by empirical approaches only because a direct structural characterization of the MQW is not possible with laboratory X-ray sources, owing to the micrometer variation of composition and thickness inherent to the SAG technique.

Based on the experience acquired in the present study, we suggest that future works on similar SAG heterostructures should be accompanied by a similar investigation of model samples, in which only the barrier (or only the well) quaternary layer is grown on the same SAG mask. In such a way, the chemical modulation of the heterostructure along the growth axis, InP[001], is absent and only the in-plane, SAG-induced, chemical modulation will be investigated. Therefore, the space-resolved chemical composition of the barrier (well) layers will be quantitatively determined by μ-XRD and μ-PL and independently cross-checked by μ-XRF.[42] To fully apply this approach to Al-containing III–V heterostructures, the adopted experimental set-up should be improved by a vacuum chamber allowing the collection of Al fluorescence at 1.5 keV.

The high cost of synchrotron radiation, together with the time needed to collect micrometer-resolved spectra and diffractograms and to process so huge an amount of data implies that this approach can not be used as routine process for quality control of SAG devices. Conversely, when the growth parameters of a new monolithic device (III–V fluxes, growth temperature, stripe composition and geometry, etc.) have to be optimized, the characterization procedure reported in the present study and in two previous reports[41,42] will provide fundamental information on how to converge faster to the ideal growth parameters for the desired device. This work represents a clear example of how academic and industrial research efforts can merge constructively.[106]

4. Experimental Section

The samples were produced in the laboratories of Avago Technologies Italy (Turin Technology Centre), with a commercial 6-inch × 2-inch Thomas Swan MOVPE reactor starting from $Al(CH_3)_3$, $Ga(CH_3)_3$, and $In(CH_3)_3$ as group-III sources, AsH_3 and PH_3 as group-V sources, and H_2 as carrier gas. The SAG growth was obtained using a SiO_2 mask with 30-µm-wide stripes and 30-µm opening widths between them (see Figure 1a). The MQW was obtained with a repetition of 9 times of the $Al_{xw}Ga_{yw}In_{1-xw-yw}As/Al_{xb}Ga_{yb}In_{1-xb-yb}As$ (compressive-strained well/tensile-strained barrier) heterostructure grown on InP. PL experiments were performed with a dispersive Scantek instrument equipped with a He–Ne excitation source (resulting in a 2-µm-diameter spot size) with a diffractive grating monochromator and an InGaAs photodetector.

The ID22 beamline exploits the radiation produced by two different undulators: a standard linear undulator (U42), covering the

© 2011 Wiley-VCH Verlag GmbH & Co. KGaA, Weinheim

energy range from 6 to 50 keV, and a second one (U23), which is a so-called in-vacuum linear undulator, inducing a much higher brilliance. Harmonic rejection is done by a single flat horizontally reflecting mirror and a Kohzu fixed-exit double-crystal monochromator is used with two different pairs of crystals: Si(111) for the low-energy range (4–37 keV, as employed in this work) and Si(311) for higher energies (7–72 keV).

The microprobe setup is based on based on the KB mirrors[97] that allowed us to reach a spatial resolution of 1.7 μm (vertical) × 5.3 μm (horizontal). The KB mirrors have an efficiency of ≈70% and, using both undulators together, when the current on the ESRF ring is ≈200 mA, the photon flux measured in the focal spot is ≈10^{12} photon s^{-1} at 13 keV. Different detectors, such as a mini-ionization chamber and a Silicon drift detector, are used to monitor the intensity of the incoming beam and XRF signals. A video microscope allows for the easy alignment of the sample and the microprobe setup.

Owing to the great number of parameters to be fitted in the EXAFS analysis of the quaternary heterostructures, we decided to put constraints exploiting data extracted by fitting XAFS spectra of reference binary GaAs and InAs samples (see Figure 7 and Table 2). The measurements of these references at the Ga and As K-edges were performed at room temperature, in transmission mode, at the GILDA beamline at the ESRF.[107] The monochromator was operated in low-flux mode with Si(311) flat crystals; the energy resolution and flux were approximately 1.2 eV and 5×10^9 photons s^{-1} on the sample, respectively, and harmonic rejection was achieved by using a pair of Pd-coated mirrors with a cutoff energy of 21 keV.

For the two reference spectra collected at the As K-edge, we performed a first-shell fit with four parameters: energy shift (ΔE_0), amplitude-reduction factor (S_0^2), As–In or As–Ga bond length ($R_{\text{As-In}}$ or $R_{\text{As-Ga}}$) and corresponding Debye–Waller factors ($\sigma^2_{\text{As-In}}$ and $\sigma^2_{\text{As-Ga}}$). For the Ga K-edge spectrum of GaAs, we extended the range in R-space up to the second shell ($R < 4.3$ Å), fitting also the Ga–Ga distance and the related Debye–Waller factor. We exploited the results obtained (reported in Table 2) to fix both the edge energies and the S_0^2 factors for the fits of the EXAFS spectra of the quaternary heterostructures (see Table 1). The interatomic distances of the binary compounds were used as starting values for the optimization of the bond lengths in the quaternary alloy to speed up the minimization process.

[1] H. J. Fan, P. Werner, M. Zacharias, *Small* **2006**, *2*, 700–717.
[2] S. A. Dayeh, D. P. R. Aplin, X. T. Zhou, P. K. L. Yu, E. T. Yu, D. L. Wang, *Small* **2007**, *3*, 326–332.
[3] M. Paladugu, J. Zou, Y. N. Guo, G. J. Auchterlonie, H. J. Joyce, Q. Gao, H. H. Tan, C. Jagadish, Y. Kim, *Small* **2007**, *3*, 1873–1877.
[4] R. Agarwal, *Small* **2008**, *4*, 1872–1893.
[5] X. Zhang, J. Zou, M. Paladugu, Y. A. Guo, Y. Wang, Y. Kim, H. J. Joyce, Q. Gao, H. H. Tan, C. Jagadish, *Small* **2009**, *5*, 366–369.
[6] C. Borschel, R. Niepelt, S. Geburt, C. Gutsche, I. Regolin, W. Prost, F. J. Tegude, D. Stichtenoth, D. Schwen, C. Ronning, *Small* **2009**, *5*, 2576–2580.
[7] G. Maruccio, C. Meyer, T. Matsui, D. V. Talapin, S. G. Hickey, H. Weller, R. Wiesendanger, *Small* **2009**, *5*, 808–812.
[8] M. Felici, P. Gallo, A. Mohan, B. Dwir, A. Rudra, E. Kapon, *Small* **2009**, *5*, 938–943.
[9] K. W. Sun, H. Y. Chang, C. M. Wang, S. Y. Wang, C. P. Lee, *Nanotechnology* **2000**, *11*, 227–232.
[10] H. Riechert, A. Y. Egorov, D. Livshits, B. Borchert, S. Illek, *Nanotechnology* **2000**, *11*, 201–205.
[11] N. N. Sibeldin, M. L. Skorikov, V. A. Tsvetkov, *Nanotechnology* **2001**, *12*, 591–596.
[12] A. A. Marmalyuk, O. I. Govorkov, A. V. Petrovsky, D. B. Nikitin, A. A. Padalitsa, P. V. Bulaev, I. V. Budkin, I. D. Zalevsky, *Nanotechnology* **2001**, *12*, 434–436.
[13] B. R. Nag, M. Das, *Nanotechnology* **2003**, *14*, 965–967.
[14] M. Esmaeili, H. Haratizadeh, B. Monemar, P. P. Paskov, P. O. Holtz, P. Bergman, M. Iwaya, S. Kamiyama, H. Amano, I. Akasaki, *Nanotechnology* **2007**, *18*, 025401.
[15] J. J. Wu, G. Y. Zhang, X. L. Liu, Q. S. Zhu, Z. G. Wang, Q. J. Jia, L. P. Guo, *Nanotechnology* **2007**, *18*, 015402.
[16] V. V. Mamutin, A. Y. Egorov, N. V. Kryzhanovskaya, *Nanotechnology* **2008**, *19*, 445715.
[17] Z. L. Fang, D. Q. Lin, J. Y. Kang, J. F. Kong, W. Z. Shen, *Nanotechnology* **2009**, *20*, 235401.
[18] M. Razeghi, *The MOCVD Challenge: Volume 2: A Survey of GaInAsP-GaAs for Photonic and Electronic Device Applications*, IoP Publishing Ltd., London **1995**.
[19] M. Gibbon, J. P. Stagg, C. G. Cureton, E. J. Thrush, C. J. Jones, R. E. Mallard, R. E. Pritchard, N. Collis, A. Chew, *Semicond. Sci. Technol.* **1993**, *8*, 998–1010.
[20] M. E. Coltrin, C. C. Mitchell, *J. Cryst. Growth* **2003**, *254*, 35–45.
[21] J. Takeda, M. Akabori, J. Motohisa, R. Notzel, T. Fukui, *Nanotechnology* **2005**, *16*, 2954–2957.
[22] L. Yang, J. Motohisa, J. Takeda, K. Tomioka, T. Fukui, *Nanotechnology* **2007**, *18*, 105302.
[23] L. Yang, J. Motohisa, J. Takeda, K. Tomioka, T. Fukui, *Nanotechnology* **2008**, *19*, 409801.
[24] N. Dupuis, J. Decobert, C. Jany, F. Alexandre, A. Garreau, N. Lagay, F. Martin, D. Carpentier, J. Landreau, C. Kazmierski, *IEEE Photonics Technol. Lett.* **2008**, *20*, 1808–1810.
[25] Z. M. Zhao, K. Yadavalli, Z. B. Hao, K. L. Wang, *Nanotechnology* **2009**, *20*, 035304.
[26] K. Tomioka, Y. Kobayashi, J. Motohisa, S. Hara, T. Fukui, *Nanotechnology* **2009**, *20*, 145302.
[27] D. Dalacu, A. Kam, D. G. Austing, X. H. Wu, J. Lapointe, G. C. Aers, P. J. Poole, *Nanotechnology* **2009**, *20*, 395602.
[28] J. Decobert, N. Dupuis, P. Y. Lagree, N. Lagay, A. Ramdane, A. Ougazzaden, F. Poingt, C. Cuisin, C. Kazmierski, *J. Cryst. Growth* **2007**, *298*, 28–31.
[29] M. Meliga, R. Paoletti, C. Coriasso, *Proc. SPIE* **2005**, *6020*, 382–391.
[30] E. Foti, L. Fratta, F. Ghiglieno, C. Coriasso, C. Cacciatore, C. Rigo, M. Agresti, M. Vallone, S. Codato, G. Fornuto, R. Fang, M. Rosso, A. Buccieri, P. Valenti, *IEEE Proc. Optoelectron.* **2004**, *151*, 103–108.
[31] R. A. Salvatore, R. T. Sahara, M. A. Bock, I. Libenzon, *IEEE J. Quantum Electron.* **2002**, *38*, 464–476.
[32] C. Henry, *IEEE J. Quantum Electron.* **1982**, *18*, 259–264.
[33] D. A. B. Miller, D. S. Chemla, T. C. Damen, *Phys. Rev. Lett.* **1984**, *53*, 2173–2176.
[34] T. Tsuchiya, J. Shimizu, M. Shirai, M. Aoki, *J. Cryst. Growth* **2003**, *248*, 384–389.
[35] G. E. Ice, *X-Ray Spectrom.* **1997**, *26*, 315–326.
[36] R. Tucoulou, G. Martinez-Criado, P. Bleuet, I. Kieffer, P. Cloetens, S. Laboure, T. Martin, C. Guilloud, J. Susini, *J. Synchrot. Radiat.* **2008**, *15*, 392–398.
[37] A. A. Sirenko, C. L. Reynolds, L. J. Peticolas, A. Ougazzaden, A. Kazimirov, R. Huang, E. Fontes, D. Bilderback, *J. Cryst. Growth* **2003**, *253*, 38–45.
[38] A. A. Sirenko, A. Kazimirov, R. Huang, D. H. Bilderback, S. O'Malley, V. Gupta, K. Bacher, L. J. P. Ketelsen, A. Ougazzaden, *J. Appl. Phys.* **2005**, *97*, 063512.
[39] A. A. Sirenko, A. Kazimirov, A. Ougazzaden, S. M. O'Malley, D. H. Bilderback, Z. H. Cai, B. Lai, R. Huang, V. K. Gupta, M. Chien, S. N. G. Chu, *Appl. Phys. Lett.* **2006**, *88*, 081111.

© 2011 Wiley-VCH Verlag GmbH & Co. KGaA, Weinheim

[40] A. A. Sirenko, A. Kazimirov, S. Cornaby, D. H. Bilderback, B. Neubert, P. Bruckner, F. Scholz, V. Shneidman, A. Ougazzaden, *Appl. Phys. Lett.* **2006**, *89*, 181926.

[41] L. Mino, D. Gianolio, G. Agostini, A. Piovano, M. Truccato, A. Agostino, S. Cagliero, G. Martinez-Criado, S. Codato, C. Lamberti, *Adv. Mater.* **2010**, *22*, 2050–2054.

[42] L. Mino, A. Agostino, S. Codato, C. Lamberti, *J. Anal. At. Spectrom.* **2010**, *25*, 831–836.

[43] M. Yoon, B. C. Larson, J. Z. Tischler, T. E. Haynes, J. S. Chung, G. E. Ice, P. Zschack, *Appl. Phys. Lett.* **1999**, *75*, 2791–2793.

[44] G. Martinez-Criado, A. Somogyi, A. Homs, R. Tucoulou, J. Susini, *Appl. Phys. Lett.* **2005**, *87*, 061913.

[45] G. Martinez-Criado, A. Segura, J. A. Sans, A. Homs, J. Pellicer-Porres, J. Susini, *Appl. Phys. Lett.* **2006**, *89*, 061906.

[46] J. A. Sans, G. Martinez-Criado, J. Pellicer-Porres, J. F. Sanchez-Royo, A. Segura, *Appl. Phys. Lett.* **2007**, *91*, 221904.

[47] G. Martinez-Criado, O. Sancho-Juan, N. Garro, J. A. Sans, A. Cantarero, J. Susini, M. Roever, D. D. Mai, A. Bedoya-Pinto, J. Malindretos, A. Rizzi, *Appl. Phys. Lett.* **2008**, *93*, 021916.

[48] M. Heuer, T. Buonassisi, M. A. Marcus, A. A. Istratov, M. D. Pickett, T. Shibata, E. R. Weber, *Phys. Rev. B* **2006**, *73*, 235204.

[49] M. Truccato, C. Lamberti, C. Prestipino, A. Agostino, *Appl. Phys. Lett.* **2005**, *86*, 213116.

[50] S. Cagliero, A. Piovano, C. Lamberti, M. M. R. Khan, A. Agostino, G. Agostini, D. Gianolio, L. Mino, J. A. Sans, C. Manfredotti, M. Truccato, *J. Synchrotron Radiat.* **2009**, *16*, 813–817.

[51] H. Bei, R. I. Barabash, G. E. Ice, W. Liu, J. Tischler, E. P. George, *Appl. Phys. Lett.* **2008**, *93*, 071904.

[52] M. Sobiech, M. Wohlschlogel, U. Welzel, E. J. Mittemeijer, W. Hugel, A. Seekamp, W. Liu, G. E. Ice, *Appl. Phys. Lett.* **2009**, *94*, 221901.

[53] W. G. Yang, B. C. Larson, G. E. Ice, J. Z. Tischler, J. D. Budai, K. S. Chung, W. P. Lowe, *Appl. Phys. Lett.* **2003**, *82*, 3856–3858.

[54] J. D. Budai, W. G. Yang, N. Tamura, J. S. Chung, J. Z. Tischler, B. C. Larson, G. E. Ice, C. Park, D. P. Norton, *Nat. Mater.* **2003**, *2*, 487–492.

[55] M. Newville, S. Sutton, M. Rivers, P. Eng, *J. Synchrotron Radiat.* **1999**, *6*, 353–355.

[56] A. Manceau, B. Lanson, M. L. Schlegel, J. C. Harge, M. Musso, L. Eybert-Berard, J. L. Hazemann, D. Chateigner, G. M. Lamble, *Am. J. Sci.* **2000**, *300*, 289–343.

[57] D. Strawn, H. Doner, M. Zavarin, S. McHugo, *Geoderma* **2002**, *108*, 237–257.

[58] F. R. Panfili, A. Manceau, G. Sarret, L. Spadini, T. Kirpichtchikova, V. Bert, A. Laboudigue, M. A. Marcus, N. Ahamdach, M. F. Libert, *Geochim. Cosmochim. Acta* **2005**, *69*, 2265–2284.

[59] A. Voegelin, S. Pfister, A. C. Scheinost, M. A. Marcus, R. Kretzschmar, *Environ. Sci. Technol.* **2005**, *39*, 6616–6623.

[60] T. A. Kirpichtchikova, A. Manceau, L. Spadini, F. Panfili, M. A. MarcuS, T. Jacquet, *Geochim. Cosmochim. Acta* **2006**, *70*, 2163–2190.

[61] J. James-Smith, J. Cauzid, D. Testemale, W. H. Liu, J. L. Hazemann, O. Proux, B. Etschmann, P. Philippot, D. Banks, P. Williams, J. Brugger, *Am. Mineral.* **2010**, *95*, 921–932.

[62] T. Itai, Y. Takahashi, T. Uruga, H. Tanida, A. Iida, *Appl. Geochem.* **2008**, *23*, 2667–2675.

[63] P. Martinetto, M. Anne, E. Dooryhee, M. Drakopoulos, M. Dubus, J. Salomon, A. Simionovici, P. Walter, *Nucl. Instrum. Meth. Phys. Res. B* **2001**, *181*, 744–748.

[64] W. S. Yue, Y. Li, X. L. Li, X. H. Yu, B. Deng, J. F. Liu, T. M. Wan, G. L. Zhang, Y. Y. Huang, W. He, W. Hua, *J. Synchrotron Radiat.* **2004**, *11*, 428–431.

[65] W. S. Yue, X. L. Lia, J. F. Liu, Y. Li, X. H. Yu, B. Deng, T. M. Wan, G. L. Zhang, Y. Y. Huang, W. He, W. Hua, L. Y. Shao, W. J. Li, S. S. Yang, *Sci. Total Environ.* **2006**, *368*, 916–925.

[66] F. Reith, B. Etschmann, C. Grosse, H. Moors, M. A. Benotmane, P. Monsieurs, G. Grass, C. Doonan, S. Vogt, B. Lai, G. Martinez-Criado, G. N. George, D. H. Nies, M. Mergeay, A. Pring, G. Southam, J. Brugger, *Proc. Natl. Acad. Sci. USA* **2009**, *106*, 17757–17762.

[67] O. Paris, I. Zizak, H. Lichtenegger, P. Roschger, K. Klaushofer, P. Fratzl, *Cell. Mol. Biol.* **2000**, *46*, 993–1004.

[68] D. V. Rao, M. Swapna, R. Cesareo, A. Brunetti, T. Akatsuka, T. Yuasa, T. Takeda, G. Tromba, G. E. Gigante, *J. Trace Elem. Med. Biol.* **2009**, *23*, 251–257.

[69] S. Yoshida, A. Ektessabi, S. Fujisawa, *J. Synchrotron Radiat.* **2001**, *8*, 998–1000.

[70] M. J. Farquharson, A. Al-Ebraheem, G. Falkenberg, R. Leek, A. L. Harris, D. A. Bradley, *Phys. Med. Biol.* **2008**, *53*, 3023–3037.

[71] S. Sanguinetti, M. Guzzi, M. Gurioli, in *Characterization of Semiconductor Heterostructures and Nanostructures* (Ed: C. Lamberti), Elsevier, Amsterdam **2008**, 175–208.

[72] C. Lamberti, *Comput. Phys. Commun.* **1996**, *93*, 82–119.

[73] C. Lamberti, *Comput. Phys. Commun.* **1996**, *93*, 53–81.

[74] C. Lamberti, S. Bordiga, F. Boscherini, S. Mobilio, S. Pascarelli, L. Gastaldi, M. Madella, C. Papuzza, C. Rigo, D. Soldani, C. Ferrari, L. Lazzarini, G. Salviati, *J. Appl. Phys.* **1998**, *83*, 1058–1077.

[75] C. Ferrari, C. Bocchi, in *Characterization of Semiconductor Heterostructures and Nanostructures* (Ed: C. Lamberti), Elsevier, Amsterdam **2008**, 93–132.

[76] S. Kimura, H. Kimura, K. Kobayashi, T. Oohira, K. Izumi, Y. Sakata, Y. Tsusaka, K. Yokoyama, S. Takeda, M. Urakawa, Y. Kagoshima, J. Matsui, *Appl. Phys. Lett.* **2000**, *77*, 1286–1288.

[77] Z. H. Cai, W. Rodrigues, P. Ilinski, D. Legnini, B. Lai, W. Yun, E. D. Isaacs, K. E. Lutterodt, J. Grenko, R. Glew, S. Sputz, J. Vandenberg, R. People, M. A. Alam, M. Hybertsen, L. J. P. Ketelsen, *Appl. Phys. Lett.* **1999**, *75*, 100–102.

[78] A. Kazimirov, A. A. Sirenko, D. H. Bilderback, Z. H. Cai, B. Lai, R. Huang, A. Ougazzaden, *J. Phys. D Appl. Phys.* **2006**, *39*, 1422–1426.

[79] N. Dupuis, J. Decobert, P. Y. Lagree, N. Lagay, C. Cuisin, F. Poingt, A. Ramdane, C. Kazmierski, *IEEE Proc. Optoelectron.* **2006**, *153*, 276–279.

[80] C. Lamberti, S. Bordiga, F. Boscherini, S. Pascarelli, G. M. Schiavini, C. Ferrari, L. Lazzarini, G. Salviati, *J. Appl. Phys.* **1994**, *76*, 4581–4586.

[81] J. C. Woicik, K. E. Miyano, J. G. Pellegrino, P. S. Shaw, S. H. Southworth, B. A. Karlin, *Appl. Phys. Lett.* **1996**, *68*, 3010–3012.

[82] J. C. Woicik, J. G. Pellegrino, B. Steiner, K. E. Miyano, S. G. Bompadre, L. B. Sorensen, T. L. Lee, S. Khalid, *Phys. Rev. Lett.* **1997**, *79*, 5026–5029.

[83] J. C. Woicik, J. A. Gupta, S. P. Watkins, E. D. Crozier, *Appl. Phys. Lett.* **1998**, *73*, 1269–1271.

[84] S. Pascarelli, F. Boscherini, C. Lamberti, S. Mobilio, *Phys. Rev. B* **1997**, *56*, 1936–1947.

[85] F. Boscherini, C. Lamberti, S. Pascarelli, C. Rigo, S. Mobilio, *Phys. Rev. B* **1998**, *58*, 10745–10753.

[86] F. Romanato, D. De Salvador, M. Berti, A. Drigo, M. Natali, M. Tormen, G. Rossetto, S. Pascarelli, F. Boscherini, C. Lamberti, S. Mobilio, *Phys. Rev. B* **1998**, *57*, 14619–14622.

[87] T. L. Lee, M. R. Pillai, J. C. Woicik, G. Labanda, P. F. Lyman, S. A. Barnett, M. J. Bedzyk, *Phys. Rev. B* **1999**, *60*, 13612–13618.

[88] M. Tormen, D. De Salvador, A. V. Drigo, F. Romanato, F. Boscherini, S. Mobilio, *Phys. Rev. B* **2001**, *63*, 115326.

[89] Y. A. Soh, G. Aeppli, F. M. Zimmermann, E. D. Isaacs, A. I. Frenkel, *J. Appl. Phys.* **2001**, *90*, 6172–6176.

[90] C. Lamberti, *Surf. Sci. Rep.* **2004**, *53*, 1–197.

[91] G. Ciatto, J. C. Harmand, F. Glas, L. Largeau, M. Le Du, F. Boscherini, M. Malvestuto, L. Floreano, P. Glatzel, R. A. Mori, *Phys. Rev. B* **2007**, *75*, 245212.

[92] M. Berti, G. Bisognin, D. De Salvador, E. Napolitani, S. Vangelista, A. Polimeni, M. Capizzi, F. Boscherini, G. Ciatto,

© 2011 Wiley-VCH Verlag GmbH & Co. KGaA, Weinheim

S. Rubini, F. Martelli, A. Franciosi, *Phys. Rev. B* **2007**, *76*, 205323.
[93] F. Boscherini, in *Characterization of Semiconductor Heterostructures and Nanostructures* (Ed: C. Lamberti), Elsevier, Amsterdam **2008**, 289–330.
[94] G. Ciatto, F. Boscherini, A. A. Bonapasta, F. Filippone, A. Polimeni, M. Capizzi, M. Berti, G. Bisognin, D. De Salvador, L. Floreano, F. Martelli, S. Rubini, L. Grenouillet, *Phys. Rev. B* **2009**, *79*, 165205.
[95] A. Rindby, *X-Ray Spectrom.* **1993**, *22*, 187–191.
[96] E. Ziegler, G. Aquilanti, O. Mathon, S. de Panfilis, P. van Vaerenbergh, *X-Ray Spectrom.* **2009**, *38*, 250–253.
[97] C. Riekel, *Rep. Progr. Phys.* **2000**, *63*, 233–262.
[98] G. Martinez-Criado, A. Somogyi, S. Ramos, J. Campo, R. Tucoulou, M. Salome, J. Susini, M. Hermann, M. Eickhoff, M. Stutzmann, *Appl. Phys. Lett.* **2005**, *86*, 131927.
[99] R. Terzano, M. Spagnuolo, L. Medici, F. Tateo, B. Vekemans, K. Janssens, P. Ruggiero, *Appl. Geochem.* **2006**, *21*, 993–1005.
[100] F. Pinakidou, M. Katsikini, E. C. Paloura, P. Kavouras, T. Kehagias, P. Komninou, T. Karakostas, A. Erko, *J. Hazard. Mater.* **2007**, *142*, 297–304.
[101] Vegard's law [L. Vegard, *Z. Phys.* **1921**, *5*, 17] allows the chemical composition of a pseudo-binary alloy to be determined from the lattice-parameter evaluation. The high crystalline quality of III–V epylayers, combined with the high angular resolution of the modern high-resolution XRD instruments allows the x composition of an $A_xB_{1-x}D$ alloy to be determined to within 0.1%. For quaternary $A_xB_{1-x}D_yE_{1-y}$ or $A_xB_yC_{1-x-y}D$ alloys, XRD measurements have to be coupled with photoluminescence to obtain the chemical composition of the epilayers, a fact that slightly increases the final incertainty in x and y. In any case, the accuracy of the chemical composition determined in this way is much higher than that achieved by EXAFS.
[102] J. C. Mikkelsen, J. B. Boyce, *Phys. Rev. B* **1983**, *28*, 7130.
[103] J. C. Mikkelsen, J. B. Boyce, *Phys. Rev. Lett.* **1982**, *49*, 1412.
[104] G. Agostini, S. Usseglio, E. Groppo, M. J. Uddin, C. Prestipino, S. Bordiga, A. Zecchina, P. L. Solari, C. Lamberti, *Chem. Mat.* **2009**, *21*, 1343–1353.
[105] F. d'Acapito, *J. Appl. Phys.* **2004**, *96*, 369–373.
[106] M. Capellas, *ESRF News* **2010**, *56*, 13.
[107] F. d'Acapito, S. Colonna, S. Pascarelli, G. Antonioli, A. Balerna, A. Bazzini, F. Boscherini, F. Campolungo, G. Chini, G. Dalba, I. Davoli, P. Fornasini, R. Graziola, G. Licheri, C. Meneghini, F. Rocca, L. Sangiorgio, V. Sciarra, V. Tullio, S. Mobilio, *ESRF Newsletter* **1998**, *30*, 42–44.

Received: July 20, 2010
Revised: December 14, 2010
Published online: March 15, 2011

© 2011 Wiley-VCH Verlag GmbH & Co. KGaA, Weinheim